

Photoinduced transition from quasi-2D Ruddlesden-Popper to 3D halide perovskites for optical writing multicolor and light-erasable images

Sergey S. Anoshkin,[†] Ivan I. Shishkin,[†] Daria I. Markina,[†] Lev S. Logunov,[†]
Hilmi Volkan Demir,^{‡,¶} Andrey L. Rogach,[§] Anatoly P. Pushkarev,^{*,†} and Sergey
V. Makarov^{*,†,||}

[†]*ITMO University, Kronverkskiy pr. 49, 197101 St. Petersburg, Russia*

[‡]*UNAM-Institute of Materials Science and Nanotechnology, National Nanotechnology
Research Center, Department of Electrical and Electronics Engineering, Department of
Physics, Bilkent University, Ankara, 06800, Turkey*

[¶]*School of Materials Science and Engineering, Nanyang Technological University,
Singapore 639798*

[§]*Department of Materials Science and Engineering and Centre for Functional Photonics
(CFP), City University of Hong Kong, 83 Tat Chee Avenue, Kowloon, Hong Kong SAR
999077, P. R. China*

^{||}*Qingdao Innovation and Development Center, Harbin Engineering University, Qingdao
266000, Shandong, P. R. China*

E-mail: anatoly.pushkarev@metalab.ifmo.ru; s.makarov@metalab.ifmo.ru

Abstract

Development of advanced optical data storage, information encryption, and security labeling technologies requires low-cost materials exhibiting local, pronounced, and diverse modification of their structure-dependent optical properties under external excitation. Herein, for these purposes, we propose and develop a novel platform relying on layered lead halide Ruddlesden-Popper (quasi-2D) phases that undergo a light-induced transition towards bulk (3D) halide perovskite and employ this phenomenon for the direct optical writing of various multicolor patterns. This transition causes the weakening of quantum confinement, and hence the bandgap reduction in these photoluminescent thin films. To significantly extend the color gamut of evolving photoluminescence, we make use of mixed-halide compositions exhibiting photoinduced halide segregation. As a result, the emission wavelength of the resulting films can be widely tuned across the entire 450–600 nm range depending on the illumination conditions. We show that pulsed near-infrared femtosecond laser irradiation provides high-resolution direct writing, whereas continuous-wave ultraviolet exposure is suitable for fast recording on larger scales. The luminescent micro- and macro-scale images created on such quasi-2D perovskite films can be erased during the visualization process, by which the persistence of these images to UV light exposure can be controlled and increased further with the increasing number of octahedral layers used in the perovskite stacks. This makes the proposed writing/erasing perovskite-based platform suitable for the manufacturing of both inexpensive optical data storage devices and light-erasable security labels.

Keywords: Ruddlesden-Popper phase, halide perovskites, phase transition, direct laser writing, light-erasable images.

Introduction

As powerful tools for the manipulation of big data, state-of-the-art technologies enabling the recording of information at nano- and micro-scales are expected to speed up progress in

natural sciences and medicine.¹⁻⁵ Also, it is profoundly beneficial if such a new technology not only affords huge capacity for data storage but also enables devices with high-level security anti-counterfeit labels. From this point of view, optical data writing applied to luminescent materials such as lead halide perovskites (LHPs) could offer solutions.⁶⁻⁹ The writing process should, however, be high-throughput and well-controlled, but at the same time hard to reproduce, without having full knowledge of the specific process.¹⁰⁻¹²

Bearing all these points in mind, the choice of laser writing on solution-processed LHP thin films could be a viable option to address the required demands. Indeed, extremely low thermal conductivity (~ 0.5 W/m·K, which is less than that of silica glasses¹³) of ABX_3 ($A = MA^+$ - methylammonium, FA^+ - formamidinium, Cs^+ ; $B = Pb^{2+}$; $X = Cl^-$, Br^- , I^-) perovskites allows for high-density optical data writing,⁸ as well as directly patterning laser microdisks, nanowire arrays^{7,14} and various micro-optical elements¹⁵⁻¹⁷ obtained by laser ablation. Moreover, photoluminescence (PL) spectral tunability over the visible spectral range can be achieved for LHPs via partial or complete substitution of a certain anion (e.g., Br^-) for another one (e.g., Cl^- or I^-) at the X site.^{18,19} Moreover, both photoinduced compositional and structural changes of the perovskite lattice could significantly impact its optical properties as well. The former has been previously demonstrated for mixed-halide perovskites revealing a phenomenon of light-driven reversible anion segregation expressed in PL redshift upon illumination and its recovery in the dark,²⁰⁻²² whereas the latter is particularly true for quasi-2D Ruddlesden-Popper (RP) phase undergoing dramatic changes in structural and optical properties under intense photoexcitation.²³⁻²⁵

Importantly, lead halide RP phase possessing $A'_2A_{n-1}Pb_nX_{3n+1}$ structure (A' - large cation, e.g., BA^+ - n-butylammonium, PEA^+ - phenethylammonium) provides the possibility of tuning the PL spectrum with an additional degree of freedom owing to the quantum confinement phenomenon in thin $[PbX_6]^{4-}$ octahedral layers separated by A' species in the perovskite stack,²⁶ whose thickness (i.e., number of the octahedral layers n) is regulated by the ratio between the corresponding halide salts employed for reaction. Concerning the data

storage applications, $(\text{PEA})_2\text{MA}_{n-1}\text{Pb}_n\text{I}_{3n+1}$ phases with $n = 1 - 5$ were utilized for recording of information in resistive random access memory (ReRAM) devices.²⁷ Besides, it was reported that the manipulation of light irradiation and gate voltage allows one to control the ion migration process and the current flow in a data storage device based on ambipolar SnO transistor with $(\text{PEA})_2\text{PbI}_4$ photoactive layer,²⁸ and, thus, to perform writing and erasing processes under illumination only. However, the use of lead halide RP phases, offering unique optical properties related to broadband spectral tunability, for all-optical data storage and labeling has not been reported to date.

In this work, we systematically study the local optical response of mixed-halide RP phases $\text{BA}_2\text{MA}_{n-1}\text{Pb}_n(\text{Br},\text{I})_{3n+1}$ ($n = 1 - 3$) to light irradiation under ambient conditions, and employ its tunability for the direct optical writing of various multicolor patterns with high resolution and broadband gamut. Quasi-2D structure of spin-coated perovskite thin films is confirmed by powder X-ray diffraction (XRD) and steady-state absorption spectroscopy. It is established that linear photoexcitation invokes almost no temporal change in the PL spectrum of $n = 1$ film, whereas $n = 2$ and $n = 3$ ones exhibit irreversible emission tunability in the 450-600 nm range. The latter is explained by light-induced compositional and structural modification of the quasi-2D phases, which experience the halide segregation, then the destruction of iodine-rich phases accompanied with I_2 release, and thereafter undergo a phase transition toward bulk MAPbBr_3 perovskite. The proposed mechanism for this observed optical response is in good agreement with *in situ* XRD measurements and tests demonstrating the I_2 release. The larger the number of octahedral layers in the perovskite stack, the more resistant the RP phase is to the aforementioned light-driven modifications. Taking all of these findings into account, as proof-of-concept demonstrations, we employ the complex behavior of evolving PL under optical irradiation in $n = 3$ film for two-photon direct laser writing (DLW) of high-resolution multicolor microimages, whereas simple projection UV lithography applied to $n = 2$ film yielded luminescent labels, which can be erased by light during the reading process. The developed writing/erasing perovskite-based platform lever-

ages on cost-efficient synthesis and fabrication, and can be employed for the manufacturing of optical data storage devices, information encryption, and security labeling.

Results and discussion

Photoinduced phase transition in Ruddlesden-Popper perovskite films. Quasi-2D mixed-halide perovskite thin films with compositions of $\text{BA}_2\text{PbBr}_2\text{I}_2$ ($n = 1$), $\text{BA}_2\text{MAPb}_2\text{Br}_3\text{I}_4$ ($n = 2$), and $\text{BA}_2\text{MA}_2\text{Pb}_3\text{Br}_4\text{I}_6$ ($n = 3$) are obtained from 0.3 M solutions of PbI_2 , methylammonium bromide (MABr) and/or n-butylammonium bromide (BABr) mixtures in anhydrous dimethyl sulfoxide (DMSO) spin-casted onto glass substrates, followed by annealing on a hot plate (for details, see *Methods*). Quasi-2D structure of the deposited films is confirmed by XRD measured in Bragg-Brentano geometry (Fig. 1a). Comparison of the recorded patterns with ones reported by Stoumpos et al.²⁹ allows us to clearly identify the number (n) of $[\text{PbX}_6]^{4-}$ octahedral layers in the perovskite-like stacks. In the $4\text{-}20^\circ$ 2θ range, the first sample shows three peaks among which the most intensive one at 6.35° corresponds to the scattering of X-ray from (002) crystallographic planes confining a single octahedral layer and double layer of BA spacer cation. According to the Bragg's law, the distance between the (002) crystallographic planes (d -spacing) equals 13.9 \AA , which is slightly shorter than that in BA_2PbI_4 ($d_{(002)}=14.2 \text{ \AA}$)²⁹ because the mixed-halide counterpart possesses a more compact crystal lattice. Introducing one and two more octahedral layers along with a required amount of MA species into the perovskite unit results in the shifting of three diffraction peaks towards small angles, as well as the appearance of additional peaks in the XRD patterns assigned to (080) and (0100) planes, respectively (Fig. 1a).

Since our study is focused on optical encryption, it is important to examine the structural evolution of any sample upon UV excitation. Therefore, *in situ* XRD measurements for the $\text{BA}_2\text{MA}_2\text{Pb}_3\text{Br}_4\text{I}_6$ film illuminated with continuous-wave UV light ($\lambda = 365 \text{ nm}$, $I = 72 \text{ mW cm}^{-2}$) for 240 min are conducted. A set of patterns collected with 40 min time interval

reveals the simultaneous descending of peaks belonging to the quasi-2D phase and their shifting towards large angles (Fig. 1b). Here it is found that the structural properties of the illuminated films do not recover in the dark conditions. Possible reasons for such irreversible behavior could be the sintering of perovskite units, divided by large cation spacer, and the loss of iodide ions promoting the formation of exclusively Br-rich structural species having smaller lattice constants as compared to that of the initial mixed-halide perovskite. Finally, all the peaks belonging to the quasi-2D phase completely disappear and the XRD pattern appears very similar to that of the bulk ($n = \infty$) cubic MAPbBr₃ exhibiting signals at 2θ of ca. 15° and 30° , which correspond to (100) and (200) planes, respectively (Fig. 1b). A complete change in the XRD patterns is complemented by optical images of the sample emitting in red at the beginning of the experiment and green at the end (Fig. S1).

The absorption spectrum of BA₂PbBr₂I₂ shows a strong exciton peak at 449 nm. With the increasing number of octahedral layers (n), this peak undergoes a bathochromic shift and becomes gradually less pronounced (Fig. 1c). The former effect is caused by the band gap narrowing due to the reduction of quantum confinement in $n = 2$ and $n = 3$ layered RP phases, along with a slight increase in the I:Br ratio (R) taking the following values: 1 for $n = 1$, ~ 1.33 for $n = 2$, and 1.50 for $n = 3$. The latter effect of the weakening of exciton oscillator strength is related to the reduction of exciton binding energy with an increase in both n and R as well. To establish some key energetic properties of the studied materials we do deconvolution of the absorption spectra by using a function describing excitonic absorption¹⁹ and, then, draw Tauc plots for band-to-band absorption (for details, see *Supporting Information*, Fig. S1). This gives us the following values for spectral broadening (Γ) and exciton binding energy (E_b), and band gap energy (E_g): for $n = 1$, $\Gamma = 0.11$ eV, $E_b = 0.22$ eV, $E_g = 2.98$ eV; for $n = 2$ – 0.07 eV, 0.17 eV, and 2.62 eV, respectively; for $n = 3$ – 0.06 eV, 0.15 eV, 2.45 eV, respectively. The descending trends for all the values with an increase in n could be explained as follows: i) increase in the number of [PbX₆]⁴⁻ octahedral layers gives more rigid structures that are more resistant to deformation of the

crystal lattice and, hence, have a reduced number of defect states scattering excitons;³⁰ ii) as the thickness of 2D structure increases, the crystal lattice field more efficiently screens photoexcited electron and hole from each other and, therefore, exciton binding energy is getting lower;³¹ iii) the reduction of quantum confinement in $n = 2$ and $n = 3$ layered phases along with the increase in the I:Br ratio results in band gap narrowing. Concerning the latter, band gap energy value for $\text{BA}_2\text{MA}_2\text{Pb}_3\text{Br}_4\text{I}_6$ ($n = 3$) is found to be much larger than that of bulk MAPbBrI_2 ($n \rightarrow \infty$) which is close to 1.8 eV.³²

Next PL spectral evolution for the samples is systematically studied upon illumination under 360 nm UV lamp with an intensity of 160 mW cm^{-2} . The films with $n = 1$ exhibit single peak green emission peaking at 500 nm that slowly shifts towards 510 nm over the whole time interval of exposure to UV light (Fig. 1d). Interestingly, here the spectral positions of this emission and the exciton absorption peak (Fig. 1c) are very different and the Stokes shift, which is supposed to be small in quasi-2D perovskites,³³ is unusually large in this case. We assume that a reasonable explanation for this observation could be an energy transfer process. In particular, we reckon that excitons formed in the phase with $n = 1$ transfer to the one with the highest n formed at grain boundaries and experience radiative recombination.^{34,35} Thus, traces of the low band gap high- n phase possibly act as excitonic funnels. Taking this into account, it is not surprising that neither the XRD patterns nor the absorption spectra demonstrate the presence of the high- n phase in the $\text{BA}_2\text{PbBr}_2\text{I}_2$ film. The films with $n = 2$ and $n = 3$ reveal similar temporal behavior of the PL signal. Initially, they emit orange light at ca. 560 nm undergoing a gradual redshift almost up to 600 nm for 1,000 s (Fig. 1e,f), with halide segregation phenomenon being responsible for such a clearly observable change.²⁰ The segregation leads to the formation of Br-rich and I-rich quasi-2D nanoscopic domains in perovskite films. The latter have a lower band gap than the former ones, and thus, takes an active part in the exciton funneling process. It should be pointed out that PL from the I-rich phase slowly deteriorates with time. This happens because of the dissociation of the I-rich domains invoked by the reaction $2\text{I}^- + 2\text{h}^+ \rightarrow \text{I}_2 (\text{g})$ describing

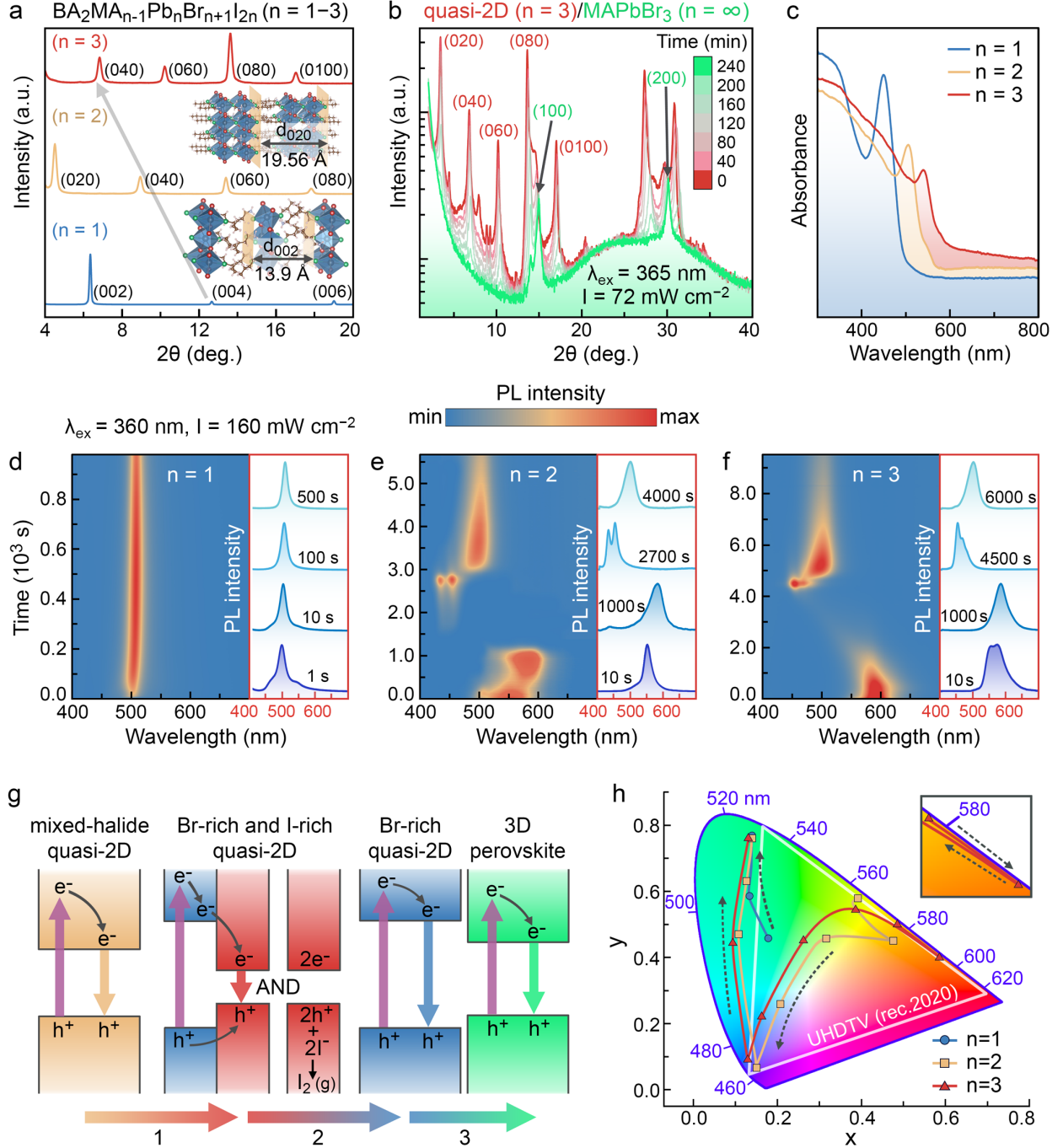


Figure 1: (a) XRD patterns of $\text{BA}_2\text{MA}_{n-1}\text{Pb}_n\text{Br}_{n+1}\text{I}_{2n}$ ($n = 1-3$) thin films. Insets illustrate crystal structure and similar crystallographic planes for $n = 1$ and $n = 2$ quasi-2D phases. The gray arrow shows an almost linear shift of the diffraction peaks towards smaller angles with increase in the number (n) of $[\text{PbX}_6]^{4-}$ octahedral layers. (b) Data derived from *in situ* XRD measurements. According to the series of patterns, $n = 3$ film undergoes phase transition from the quasi-2D structure to bulk MAPbBr_3 ($n = \infty$) upon continuous-wave UV excitation ($I = 72 \text{ mW cm}^{-2}$) for 240 min. (c) Absorption spectra for the $n = 1-3$ RP films.

(d-f) Evolution of PL spectra in the films with $n = 1 - 3$ exposed to 360 nm light with intensity of 160 mW cm^{-2} . The $n = 1$ film shows exclusively green emission from the grain boundaries, whereas $n = 2$ and $n = 3$ films demonstrate remarkable spectral tuning of PL color. (g) Energy diagram depicting the possible mechanism for spectral tuning in the $n = 2$ and $n = 3$ films. Three types of compositional and structural transformation are indicated with gradient arrows: 1) light-induced halide segregation invoking Br- and I-rich quasi-2D phases; 2) I_2 release-assisted dissociation of the I-rich phase and 3) sintering of Br-rich quasi-2D phase resulting in the formation of 3D bromide perovskite. (h) CIE 1931 color space exhibiting the change of PL color corresponding to the dynamics plotted in (d)-(f).

the generation of a volatile iodine species via the oxidation of iodide ions by photoexcited holes (h^+) in the valence band of perovskites.³⁶ To find evidence of such a dissociation mechanism, the $n = 3$ $\text{BA}_2\text{MA}_2\text{Pb}_3\text{Br}_4\text{I}_6$ film encapsulated together with a small piece of a KI test paper is illuminated until the complete deterioration of the reddish-orange luminescence (Fig. S3). One can see that the released I_2 gas reacts with KI, giving a darkened edge of the test paper beside the area of the film exposed to UV light for 100 min (bottom image in Fig. S3). When the I-rich domains are finally depleted, exciton radiative recombination occurs within the Br-rich ones. Therefore, for $n = 2$ film, we observe a peak at 434 nm assigned to $\text{BA}_2\text{MAPb}_2\text{Br}_7$ ²⁴ accompanied with the second peak at 454 nm, most likely related to the emission from hollow perovskite structures³⁷ containing large BA cations sealed in MAPbBr_3 crystal lattice. These hollow perovskites are an intermediate of the sintering process, which are formed as a result of the evolution of $n = 3$ film, along with the second less pronounced emission peaked at 468 nm belonging to $\text{BA}_2\text{MA}_2\text{Pb}_3\text{Br}_{10}$ phase.³⁵ Finally, blue emission in both $n = 2$ and $n = 3$ films changes to green, which occurs within the Br-rich quasi-2D domains due to the sintering process and results in the formation of phases with larger n and finally bulk MAPbBr_3 ($n = \infty$) in the end. To illustrate the above discussion, a qualitative energy diagram (Fig. 1g) visualizes three key stages during the evolution of PL color governed by the aforementioned UV light-induced structural transformations $n = 2$ and $n = 3$ perovskite films.

To find more evidence of the proposed mechanism we demonstrate synchronous absorption-

PL dynamics for all the films (Fig. S4). First, we measure the initial absorption spectra for them and, then, they are illuminated by UV light ($\lambda_{ex} = 360$ nm, $I = 160$ mW cm⁻²) for obtaining PL dynamics. By interrupting the exposure of the films to UV light at certain moments and measuring absorption spectra for them consistent data on absorption and PL dynamics are collected. It is established that $n = 1$ film exhibits the following changes in its absorption spectrum (Fig. S4a): i) the absorption peak at 449 nm goes down and undergoes a blueshift; ii) a shoulder appears in the 500-520 nm range and further evolves into a pronounced peak at 510 nm; iii) a new peak at ca. 400 nm arises. The first two observations are in good agreement with the halide segregation phenomenon, dissociation of the I-rich phase due to the release of I₂ species, and the formation of bulk perovskite, whereas the third one can be explained by the formation of BA₂PbBr₄ phase exhibiting its own excitonic absorption.³⁸ Concerning the PL dynamics for $n = 1$ (Fig. S4b), we emphasize it is not capable of giving clear information about structural transformations because long-range exciton transport in quasi-2D perovskites³³ and efficient energy funneling phenomena³⁹ results in photoluminescence of the bulk phase impurity evenly distributed in the film. On the contrary, absorption and PL dynamics for $n = 2$ and $n = 3$ look quite consistent. In particular, after the halide segregation and dissociation of the I-rich phase, in both absorption and PL spectra the peaks assigned to BA₂MAPb₂Br₇ ($\lambda_{abs} = 430$ nm and $\lambda_{em} = 434$ nm for $n = 2$ film in Fig. S4c,d)³⁸ and, most likely, to hollow perovskite structures ($\lambda_{abs} = 450$ nm and $\lambda_{em} = 454$ nm for $n = 2$ and $n = 3$ films in Fig. S4c-f)³⁷ can be clearly identified.

The evolution of PL spectra for the studied thin films can be well captured and conveniently represented in the form of shifting emission color coordinates according to CIE 1931 color space diagram (Fig. 1h). While the sample with $n = 1$ shows no significant color change, PL color for $n = 2$ and $n = 3$ films start from yellow ($x = 0.395$, $y = 0.557$) and orange ($x = 0.559$, $y = 0.435$), moving to purple ($x = 0.167$, $y = 0.110$) and blue ($x = 0.131$, $y = 0.096$), and, finally, turn to the same green color ($x = 0.141$, $y = 0.775$), respectively, on the color gamut. It should be noted, that both of these phases experience segregation-driven

color change expressed in the saturated orange hues ($x = 0.441$, $y = 0.476$) for $n = 2$ and ($x = 0.591$, $y = 0.402$) for $n = 3$ at the initial stage of excitation. It is important that the $n = 3$ phase displays the widest color span which extends beyond the rec. 2020 (UHDTV) color space and, hence, is preferable for the production of optical data storage devices as well as for the optical writing of anti-counterfeit images. The $n = 2$ phase undergoes faster spectral evolution as compared to the former one and could provide optical images with an additional degree of security related to the limited number of reading cycles. In the following, we will demonstrate the realization of the both opportunities.

Direct laser writing of multicolor micro-images. Experimental data on the evolution of PL color for the $n = 3$ quasi-2D perovskite films upon prolonged UV-light illumination (see Fig. 1h) inspires and justifies their applicability to the production of multicolor PL patterns through the spatially resolved automatic management of irradiation dose (fluence). One of the state-of-the-art techniques for the creation of such patterns is direct laser writing (DLW),⁸ schematically illustrated in Figure 2a. To implement DLW on the $n = 3$ phase, we employ a lithography setup (for details, see *Methods*) based on a femtosecond pulsed Ti:sapphire laser ($\lambda_{ex} = 790$ nm, $\tau = 100$ fs, $f = 80$ MHz). Using this DLW system, the aforementioned photoinduced structural transformation from the quasi-2D to 3D perovskite phase occurs because of the two-photon absorption phenomenon in the near-infrared range.⁴⁰ The control over the irradiation dose can conveniently be exercised by varying two parameters - intensity of the optical excitation and duration of the film exposure to laser pulses. The dynamic range (DR) for the dosage is established as follows: at an intensity varying from 1.24×10^7 up to 1.47×10^7 W cm⁻², the time interval of exposure varies in the range of 2.0–3.9 ms and subsequently the optimal set of produced luminescent pixels is selected (Fig. 2b). Inspection of a whole array of the pixels depicted in Figure 2b reveals that the optimal DR spans from 2.86×10^4 to 5.75×10^4 J cm⁻², as this range does not result in any burnt (overexposed) or poorly resolved (underexposed) pixels.

Thereafter, we conduct the dots per inch (DPI) test to evaluate the maximum capacity of

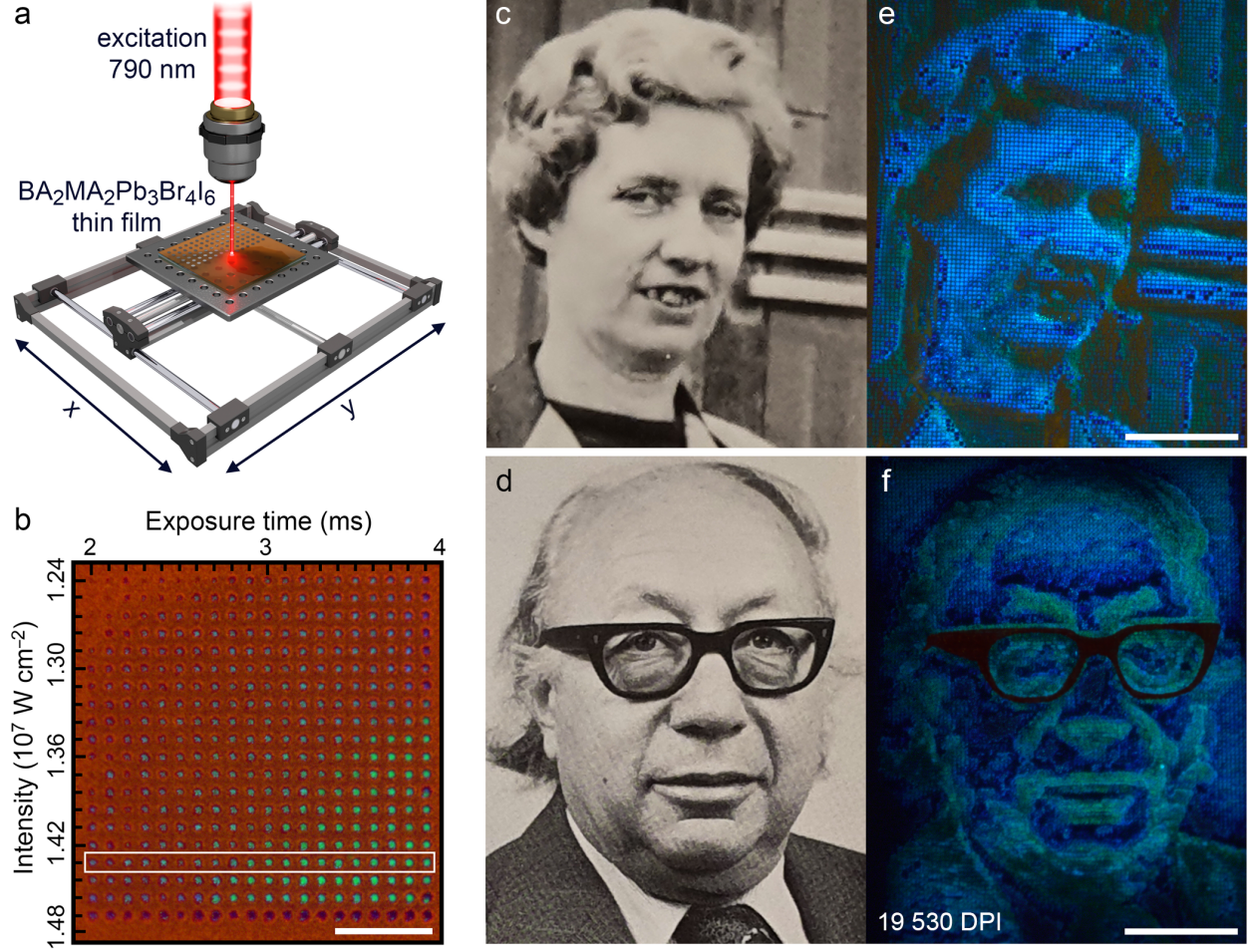


Figure 2: (a) Schematic illustration of two-photon direct laser writing (DLW) procedure applied to $n = 3$ quasi-2D perovskite thin film. (b) Luminescent image of an array of microspots preliminary exposed to various intensities of 790-nm pulsed laser irradiation for various time intervals (scale bar is $50 \mu\text{m}$). A white box identifies an optimal dynamic range for DLW giving the widest PL color gamut with no burnt (overexposed) or poorly resolved (underexposed) spots. (c-f) Original pictures of Dr. S. Ruddlesden (c) and Prof. P. Popper (d) chosen for the production of corresponding high-resolution (19500 DPI) multicolor luminescent micro-images (e,f) by using DLW method (scale bar is $50 \mu\text{m}$).

information produced by DLW procedure. A bright-field micro-image (Fig. S5a) visualizing a set of 2×2 dot patterns reveals that the dots with a diameter of $1 \mu\text{m}$ can be spatially resolved when the distance between their centers is equal to $1.6 \mu\text{m}$. This provides us with a maximum resolution of ca. 19500 DPI a resolution at which we show the construction of a simple quick response (QR) code consisting of pixels emitting the same blue light (Fig. S5b,c). The maximum resolution is also further used for the creation of complex multicolor

micro-images.

To demonstrate the applicability of the $n = 3$ perovskite film to the optical data storage and anti-counterfeit labeling, two black and white pictures of the discoverers of the quasi-2D phase Dr. Sheila Ruddlesden and Prof. Paul Popper (Fig. 2c,d) are reproduced on a micro-scale. For this purpose, their photos are digitized and then downsampled to 20 shades of gray. Pixels possessing the lightest shade specify the regions to be subjected to the highest irradiation dose for parts of the film resulting in a green color of PL, whereas the ones with the darkest shade indicated the unexposed area exhibiting a reddish-orange PL. The rest of the shades set up a linear increment of the fluence in the $0-5.75 \times 10^4 \text{ J cm}^{-2}$ range. As a result, corresponding multicolor high-resolution fluorescence images are formed (Fig. 2d,f). These images provide reasonable examples of high-capacity optical data storage, since each of the 20 shades encodes the corresponding PL spectrum, which could be assigned to a certain binary number. Furthermore, the spatial distribution of the resultant luminescent pixels makes it possible to consider such images as micro-scale anti-counterfeit labels.

Projection optical lithography of light-erasable micro-images. Following the trend of technological diversification for manufacturing luminescent micro-labels, we examine a simple projection optical lithography (POL) instead of DLW. For this purpose, a mask with a logotype of ITMO University consisting of a patterned aluminum film on a glass substrate is mounted before a $50\times$ objective and shades a continuous-wave beam of UV light at 360 nm projected on the top of the $n = 2$ quasi-2D film (Fig. 3a). At the incident light intensity of 3.5 W cm^{-2} , the illuminated area shown in Figure 3b becomes blue in the center after 120 s because of the uneven lateral distribution of the irradiation. After the mask removal, unexposed regions exhibit yellow luminescence and turn blue as well after 60 s of illumination (Fig. 3c). Remarkably, more prolonged exposure to the UV light (longer than 120 s) causes erasing of the label manifested in the appearance of a green spot undergoing the temporal lateral propagation (Fig. 3c). The control over time intervals for writing and erasing steps can be realized by tuning both the excitation intensity and thickness of the

studied quasi-2D film. Such behavior of the $n = 2$ phase is favorable for advanced security labeling^{41,42} which limits the number of label examination acts to only a few or even just one, making it invalid for further reading.

Long-term stability of luminescent patterns. Finally, we study the resistance of encapsulated micro-images and films to photobleaching caused by long-lasting light exposure to evaluate their applicability for storage on the shelf. For this purpose, a micro-image encapsulated at ambient conditions (relative humidity 35%) by using a double-sided tape and coverslip of 150 μm thickness is aged on a windowsill for 1 month. Thus, it is exposed to indoor lighting and direct sunlight in an ad hoc fashion at temperature varying in the 20–40 $^{\circ}\text{C}$ range. A comparison of pictures taken of the as-prepared micro-image and the aged one shows no significant change (Fig. S6a,b). Furthermore, we measure absorption and PL spectral dynamics for encapsulated at the same conditions $n = 3$ thin film illuminated by continuous wave UV light ($\lambda_{ex} = 365 \text{ nm}$, $I = 80 \text{ mW cm}^{-2}$) for 600 min (Fig. S6c,d). It is established that the encapsulated sample demonstrates the slowing down of the spectral dynamics by more than 40 times as compared to that of non-encapsulated one irradiated by two times more intensive light (Fig. S4e,f). Importantly, spectral dynamics for $n = 3$ film encapsulated with KI test paper is about 15 faster than that of one without it (Fig. S7). We assume the reason for such a drastic difference in dynamics stems from the ability of released I_2 species to react with the film and, hence, to slow down the conversion of mixed-halide quasi-2D phase into pure bromide quasi-2D one. Therefore, in the presence of KI test paper absorbing I_2 the conversion goes faster. Thus, I_2 release process is recognized to be responsible for the most pronounced change in PL color of our samples. A further change in PL color caused by the light-induced transition from pure bromide quasi-2D phase to bulk perovskite could be oxygen- or/and moisture-assisted as well as the thermally-assisted process. Considering all this, one can see how even a very simple encapsulation procedure substantially increases the temporal stability of the luminescent micro-images and films and provides them with an opportunity for commercialization.

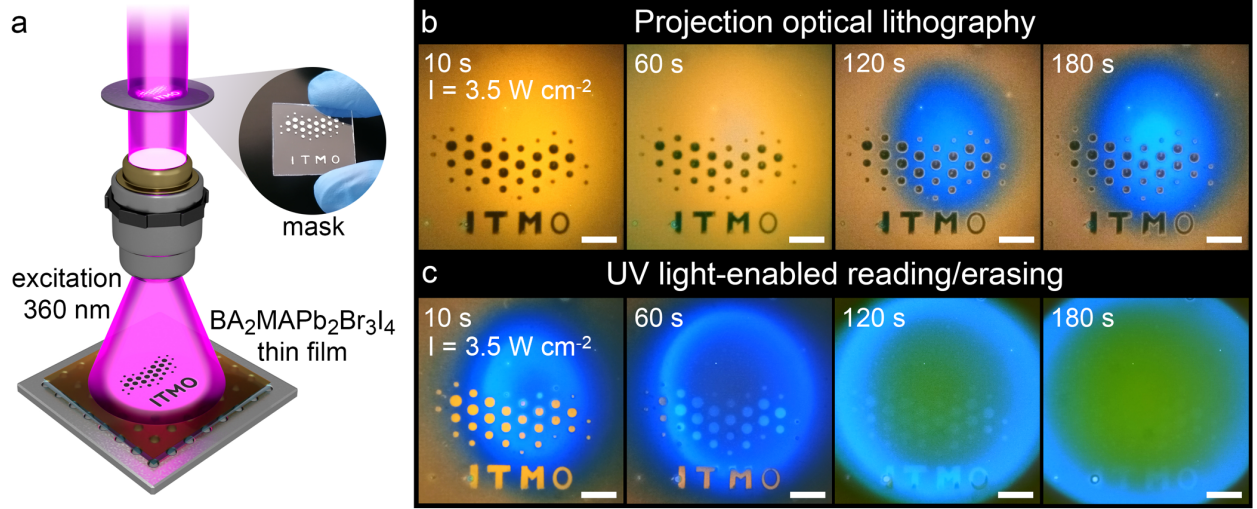


Figure 3: (a) Schematic illustration of the projection optical lithography procedure applied to the $n = 2$ quasi-2D perovskite thin film. (b) Luminescent images of the area exposed through a mask (with a logotype of ITMO University) to focused UV light with intensity of 3.5 W cm^{-2} for 10, 60, 120, and 180 s (scale bar is $50 \mu\text{m}$). Black areas are shaded with the mask. Note that a blue luminescent spot appears in the center of the area because of uneven distribution of the incident light intensity over the field of view. (c) Luminescent images of the same area after the mask removal upon the same photoexcitation for 10, 60, 120, and 180 s. In the beginning of visualization process, a contrast yellow pattern within the blue spot is revealed, which gradually disappears over time and, finally, turns to green.

Conclusions

In summary, we have demonstrated the light-induced PL emission tuning of BA₂MA _{$n-1$} Pb _{n} (Br,I) _{$3n+1$} ($n = 2, 3$) thin films. The mechanisms for such spectral tuning in the studied mixed-halide quasi-2D Ruddlesden-Popper perovskites involve irreversible compositional and structural modifications, which go beyond the conventional halide segregation in 3D (bulk) perovskites. It has been established that the $n = 3$ film is more resistant to light-driven transition from the quasi-2D phase to the 3D bulk phase, as compared to $n = 2$ film. This has allowed us to create high-resolution multicolor micro-images on the $n = 3$ quasi-2D perovskite thin films using a two-photon direct laser writing method by controlling the irradiation dose and exposure time. These images can be considered as examples of high-capacity optical data storage, and could meet the demands of information encryption technology, which significantly overcomes previous works on halide perovskites in terms of DPI.^{43–45} Moreover, a

simple projection UV lithography has been applied to the $n = 2$ quasi-2D perovskite films to demonstrate light-erasable luminescent labels, which may provide secure items with an advanced level of protection and speed up the potential progress in anti-counterfeiting.

Methods

Fabrication of quasi-2D perovskite thin films. Lead halide RP phase precursor solutions were obtained by mixing 138.3 mg (0.3 mmol) of lead(II) iodide (PbI_2 , TCI, 99.99%, trace metals basis) with the corresponding amounts of methylammonium bromide (MABr, Greatcell Solar, 99.99%) and/or n-butylammonium bromide (BABr, Greatcell Solar, 98%), and dissolution of the mixtures in 1 mL of anhydrous dimethyl sulfoxide (DMSO, Sigma-Aldrich, 99.9%). For $\text{BA}_2\text{PbBr}_2\text{I}_2$ ($n = 1$) solution, 92.4 mg (0.6 mmol) of BABr was used. For $\text{BA}_2\text{MAPb}_2\text{Br}_3\text{I}_4$ ($n = 2$) solution, 46.2 mg (0.3 mmol) of BABr and 16.8 mg (0.15 mmol) of MABr were employed. For $\text{BA}_2\text{MA}_2\text{Pb}_3\text{Br}_4\text{I}_6$ ($n = 3$) solution, 30.8 mg (0.2 mmol) of BABr and 22.4 mg (0.2 mmol) of MABr were used. Glass substrates were cleaned by subsequent ultrasonication in acetone and 2-propanol, rinsed with deionized water and exposed to ozone treatment for 10 min in order to improve wettability of the surface. The precursor solutions were spin-casted on the substrates at 2,500 rpm for 5 min and then annealed on a hot plate at 60 °C for 5 min. The thickness of the resultant thin films was 60 nm. All the procedures were conducted inside a N_2 -filled glove box with both O_2 and H_2O concentrations (not exceeding 1 ppm).

Characterization of thin films. Thickness of the deposited films was measured by using a Tencor P-7 stylus profilometer (KLA). Optical absorption spectra were recorded using a UV-3600 spectrophotometer (Shimadzu). XRD patterns of the samples were measured in $\theta - \theta$ geometry on a SmartLab diffractometer (Rigaku) equipped with a 9 kW rotating Cu anode X-ray tube. Bright-field and fluorescence images of the samples were obtained on Axio Imager A2m (Carl Zeiss) microscope with 50 \times and 100 \times objectives (Carl Zeiss EC

Epiplan-NEOFLUAR). Evolution of PL spectra was recorded by using a QE Pro optical fiber spectrometer (Ocean Optics) coupled with the microscope in the fluorescence mode.

Direct laser writing. For creating various micro-patterns on the perovskite film surface, direct laser writing (DLW) technique was applied. Laser pulses of duration 100 fs from a Ti-sapphire oscillator emitting at a wavelength of 790 nm with a repetition rate of 80 MHz were focused through a 40 \times objective (NA=0.7) onto the quasi-2D perovskite film surface. The irradiation power was monitored by thermopile sensor and controlled by a motorized half-wave plate ($\lambda/2$) and a polarizing beamsplitter. The exposure time was controlled by acousto-optical modulator used as a fast laser shutter. The positioning of the sample was performed by air bearing linear motor stages (Aerotech). DLW was conducted at ambient conditions (relative humidity 35%).

Projection UV optical lithography. A thin-film (100 nm) metal pattern on a glass substrate was fabricated by thermal evaporation of aluminum pellets (Ted Pella, Inc, 99.999%) with a deposition rate of 0.3 nm \cdot s $^{-1}$ in a vacuum chamber (Kurt J Lesker Company) at 2×10^{-7} Torr pressure. The obtained mask with a logotype of ITMO University was mounted on the microscope instead of an aperture-adjustable optical iris diaphragm in front of HBO 100 W/2 mercury short-arc lamp (OSRAM). Optical power of the focused incident UV light was measured with a Star Bright power meter (Ophir Photonics). Projection UV optical lithography was conducted at ambient conditions (relative humidity 35%).

Acknowledgement

This research was supported by Priority 2030 Federal Academic Leadership Program and by the Ministry of Science and Higher Education of the Russian Federation (Project 075-15-2021-589), and by the Croucher Foundation of Hong Kong SAR. HVD gratefully acknowledges support from TUBA. The authors thank Dr. Vidas Pakštas for measuring XRD patterns (Fig. 1b). The authors are grateful to Ann Pace (Lucideon Ltd.) for providing

them with pictures of Dr. S. Ruddlesden and Prof. P. Popper. The authors thank Mr. Ivan Pustovit for assistance in graphic design.

Supporting Information Available

Photographs of $n = 3$ quasi-2D perovskite film at the beginning and end of *in situ* XRD measurement, pictures of $n = 3$ film examined for I₂ gas release, bright-field and luminescence micro-images of 2×2 dots patterns and high-resolution QR code produced by using two-photon direct laser writing method.

References

- (1) Tsai, W.-P.; Feng, D.; Pan, M.; Beck, H.; Lawson, K.; Yang, Y.; Liu, J.; Shen, C. From Calibration to Parameter Learning: Harnessing the Scaling Effects of Big Data in Geoscientific Modeling. *Nat. Commun.* **2021**, *12*, 5988.
- (2) Lemm, D.; von Rudorff, G. F.; von Lilienfeld, O. A. Machine Learning Based Energy-Free Structure Predictions of Molecules, Transition States, and Solids. *Nat. Commun.* **2021**, *12*, 4468.
- (3) Plata, D. L.; Janković, N. Z. Achieving Sustainable Nanomaterial Design Through Strategic Cultivation of Big Data. *Nat. Nanotechnol.* **2021**, *16*, 612–614.
- (4) Lee, B.; Yoon, S.; Lee, J. W.; Kim, Y.; Chang, J.; Yun, J.; Ro, J. C.; Lee, J.-S.; Lee, J. H. Statistical Characterization of The Morphologies of Nanoparticles Through Machine Learning Based Electron Microscopy Image Analysis. *ACS Nano* **2020**, *14*, 17125–17133.
- (5) Jiang, P.; Sinha, S.; Aldape, K.; Hannenhalli, S.; Sahinalp, C.; Rupp, E. Big Data in Basic and Translational Cancer Research. *Nat. Rev. Cancer* **2022**, 1–15.

- (6) Huang, X.; Guo, Q.; Yang, D.; Xiao, X.; Liu, X.; Xia, Z.; Fan, F.; Qiu, J.; Dong, G. Reversible 3D Laser Printing of Perovskite Quantum Dots Inside a Transparent Medium. *Nat. Photon.* **2020**, *14*, 82–88.
- (7) Zhizhchenko, A. Y.; Tonkaev, P.; Gets, D.; Larin, A.; Zuev, D.; Starikov, S.; Pustovalov, E. V.; Zakharenko, A. M.; Kulinich, S. A.; Juodkasis, S.; Kuchmizhak, A. A.; Makarov, S. V. Light-Emitting Nanophotonic Designs Enabled by Ultrafast Laser Processing of Halide Perovskites. *Small* **2020**, *16*, 2000410.
- (8) Zhan, W.; Meng, L.; Shao, C.; Wu, X.-g.; Shi, K.; Zhong, H. In Situ Patterning Perovskite Quantum Dots by Direct Laser Writing Fabrication. *ACS Photonics* **2021**, *8*, 765–770.
- (9) Sun, K.; Tan, D.; Fang, X.; Xia, X.; Lin, D.; Song, J.; Lin, Y.; Liu, Z.; Gu, M.; Yue, Y.; Qiu, J. Three-Dimensional Direct Lithography of Stable Perovskite Nanocrystals in Glass. *Science* **2022**, *375*, 307–310.
- (10) Cheng, C.-H.; Yang, D. S.; Kim, J.; Deotare, P. B. Self-Erasable and Rewritable Optoexcitonic Platform for Antitamper Hardware. *Adv. Opt. Mater.* **2020**, *8*, 2001287.
- (11) Gong, X.; Qiao, Z.; Liao, Y.; Zhu, S.; Shi, L.; Kim, M.; Chen, Y.-C. Enzyme-Programmable Microgel Lasers for Information Encoding and Anti-Counterfeiting. *Adv. Mater.* **2022**, *34*, 2107809.
- (12) Larin, A. O.; Dvoretckaia, L. N.; Mozharov, A. M.; Mukhin, I. S.; Cherepakhin, A. B.; Shishkin, I. I.; Ageev, E. I.; Zuev, D. A. Luminescent Erbium-Doped Silicon Thin Films for Advanced Anti-Counterfeit Labels. *Adv. Mater.* **2021**, *33*, 2005886.
- (13) Haeger, T.; Heiderhoff, R.; Riedl, T. Thermal Properties of Metal-Halide Perovskites. *J. Mater. Chem. C* **2020**, *8*, 14289–14311.

- (14) Zhizhchenko, A.; Syubaev, S.; Berestennikov, A.; Yulin, A. V.; Porfirev, A.; Pushkarev, A.; Shishkin, I.; Golokhvast, K.; Bogdanov, A. A.; Zakhidov, A. A.; Kuchmizhak, A. A.; Kivshar, Y. S.; Makarov, S. V. Single-Mode Lasing from Imprinted Halide-Perovskite Microdisks. *ACS Nano* **2019**, *13*, 4140–4147.
- (15) Zhizhchenko, A.; Cherepakhin, A.; Masharin, M.; Pushkarev, A.; Kulinich, S.; Porfirev, A.; Kuchmizhak, A.; Makarov, S. Direct Imprinting of Laser Field on Halide Perovskite Single Crystal for Advanced Photonic Applications. *Laser Photon. Rev.* **2021**, *15*, 2100094.
- (16) Zhizhchenko, A. Y.; Cherepakhin, A. B.; Masharin, M. A.; Pushkarev, A. P.; Kulinich, S. A.; Kuchmizhak, A. A.; Makarov, S. V. Directional Lasing from Nanopatterned Halide Perovskite Nanowire. *Nano Lett.* **2021**, *21*, 10019–10025.
- (17) Wang, Z.; Yang, T.; Zhang, Y.; Ou, Q.; Lin, H.; Zhang, Q.; Chen, H.; Hoh, H. Y.; Jia, B.; Bao, Q. Flat Lenses Based on 2D Perovskite Nanosheets. *Adv. Mater.* **2020**, *32*, 2001388.
- (18) Protesescu, L.; Yakunin, S.; Bodnarchuk, M. I.; Krieg, F.; Caputo, R.; Hendon, C. H.; Yang, R. X.; Walsh, A.; Kovalenko, M. V. Nanocrystals of Cesium Lead Halide Perovskites (CsPbX_3 , $\text{X} = \text{Cl, Br, and I}$): Novel Optoelectronic Materials Showing Bright Emission with Wide Color Gamut. *Nano Lett.* **2015**, *15*, 3692–3696.
- (19) Liashenko, T. G.; Cherotchenko, E. D.; Pushkarev, A. P.; Pakštas, V.; Naujokaitis, A.; Khubezhov, S. A.; Polozkov, R. G.; Agapev, K. B.; Zakhidov, A. A.; Shelykh, I. A.; Makarov, S. V. Electronic Structure of $\text{CsPbBr}_{3-x}\text{Cl}_x$ Perovskites: Synthesis, Experimental Characterization, and DFT Simulations. *Phys. Chem. Chem. Phys.* **2019**, *21*, 18930–18938.
- (20) Hoke, E. T.; Slotcavage, D. J.; Dohner, E. R.; Bowring, A. R.; Karunadasa, H. I.;

- McGehee, M. D. Reversible Photo-Induced Trap Formation in Mixed-Halide Hybrid Perovskites for Photovoltaics. *Chem. Sci.* **2015**, *6*, 613–617.
- (21) Brennan, M. C.; Draguta, S.; Kamat, P. V.; Kuno, M. Light-Induced Anion Phase Segregation in Mixed Halide Perovskites. *ACS Energy Lett.* **2017**, *3*, 204–213.
- (22) Knight, A. J.; Wright, A. D.; Patel, J. B.; McMeekin, D. P.; Snaith, H. J.; Johnston, M. B.; Herz, L. M. Electronic Traps and Phase Segregation in Lead Mixed-Halide Perovskite. *ACS Energy Lett.* **2018**, *4*, 75–84.
- (23) Ha, S. K.; Mauck, C. M.; Tisdale, W. A. Toward stable deep-blue luminescent colloidal lead halide perovskite nanoplatelets: systematic photostability investigation. *Chemistry of Materials* **2019**, *31*, 2486–2496.
- (24) Leung, T. L.; Tam, H. W.; Liu, F.; Lin, J.; Ng, A. M. C.; Chan, W. K.; Chen, W.; He, Z.; Lončarić, I.; Grisanti, L.; Ma, C.; Wong, K. S.; Lau, Y. S.; Zhu, F.; Skoko, Ž.; Popović, J.; Djurišić, A. B. Mixed Spacer Cation Stabilization of Blue-Emitting n=2 Ruddlesden–Popper Organic–Inorganic Halide Perovskite Films. *Adv. Opt. Mater.* **2020**, *8*, 1901679.
- (25) Sen, A.; Chatterjee, S.; Sen, P. UV-Assisted Conversion of 2D Ruddlesden–Popper Iodide Perovskite Nanoplates into Stable 3D MAPbI₃ Nanorods. *The Journal of Physical Chemistry C* **2022**, *126*, 18057–18066.
- (26) Gan, Z.; Cheng, Y.; Chen, W.; Loh, K. P.; Jia, B.; Wen, X. Photophysics of 2D Organic–Inorganic Hybrid Lead Halide Perovskites: Progress, Debates, and Challenges. *Adv. Sci.* **2021**, *8*, 2001843.
- (27) Solanki, A.; Guerrero, A.; Zhang, Q.; Bisquert, J.; Sum, T. C. Interfacial Mechanism for Efficient Resistive Switching in Ruddlesden–Popper Perovskites for Non-Volatile Memories. *J. Phys. Chem. Lett.* **2019**, *11*, 463–470.

- (28) Tian, Q.; Hong, R.; Liu, C.; Hong, X.; Zhang, S.; Wang, L.; Lv, Y.; Liu, X.; Zou, X.; Liao, L. Flexible SnO Optoelectronic Memory Based on Light-Dependent Ionic Migration in Ruddlesden–Popper Perovskite. *Nano Lett.* **2021**, *22*, 494–500.
- (29) Stoumpos, C. C.; Cao, D. H.; Clark, D. J.; Young, J.; Rondinelli, J. M.; Jang, J. I.; Hupp, J. T.; Kanatzidis, M. G. Ruddlesden–Popper Hybrid Lead Iodide Perovskite 2D Homologous Semiconductors. *Chem. Mater.* **2016**, *28*, 2852–2867.
- (30) Cortecchia, D.; Neutzner, S.; Srimath Kandada, A. R.; Mosconi, E.; Meggiolaro, D.; De Angelis, F.; Soci, C.; Petrozza, A. Broadband emission in two-dimensional hybrid perovskites: the role of structural deformation. *Journal of the American Chemical Society* **2017**, *139*, 39–42.
- (31) Chernikov, A.; Berkelbach, T. C.; Hill, H. M.; Rigosi, A.; Li, Y.; Aslan, B.; Reichman, D. R.; Hybertsen, M. S.; Heinz, T. F. Exciton binding energy and nonhydrogenic Rydberg series in monolayer WS₂. *Physical review letters* **2014**, *113*, 076802.
- (32) Cui, D.; Yang, Z.; Yang, D.; Ren, X.; Liu, Y.; Wei, Q.; Fan, H.; Zeng, J.; Liu, S. Color-tuned perovskite films prepared for efficient solar cell applications. *The Journal of Physical Chemistry C* **2016**, *120*, 42–47.
- (33) Deng, S.; Shi, E.; Yuan, L.; Jin, L.; Dou, L.; Huang, L. Long-Range Exciton Transport and Slow Annihilation in Two-Dimensional Hybrid Perovskites. *Nat. Commun.* **2020**, *11*, 1–8.
- (34) Qin, Z.; Dai, S.; Gajjela, C. C.; Wang, C.; Hadjiev, V. G.; Yang, G.; Li, J.; Zhong, X.; Tang, Z.; Yao, Y.; Guloy, A. M.; Reddy, R.; Mayerich, D.; Deng, L.; Yu, Q.; Feng, G.; Calderon, H. A.; Robles-Hernandez, F. C.; Wang, Z. M.; Bao, J. Spontaneous Formation of 2D/3D Heterostructures on the Edges of 2D Ruddlesden–Popper Hybrid Perovskite Crystals. *Chem. Mater.* **2020**, *32*, 5009–5015.

- (35) Qin, Y.; Li, Z.-G.; Gao, F.-F.; Chen, H.; Li, X.; Xu, B.; Li, Q.; Jiang, X.; Li, W.; Wu, X.; Quan, Z.; Ye, L.; Zhang, Y.; Lin, Z.; Pedesseau, L.; Even, J.; Lu, P.; Bu, X.-H. Dangling Octahedra Enable Edge States in 2D Lead Halide Perovskites. *Adv. Mater.* **2022**, 2201666.
- (36) Brennan, M. C.; Toso, S.; Pavlovetc, I. M.; Zhukovskyi, M.; Marras, S.; Kuno, M.; Manna, L.; Baranov, D. Superlattices are Greener on the Other Side: How Light Transforms Self-Assembled Mixed Halide Perovskite Nanocrystals. *ACS Energy Lett.* **2020**, 5, 1465–1473.
- (37) Worku, M.; Tian, Y.; Zhou, C.; Lin, H.; Chaaban, M.; Xu, L.-j.; He, Q.; Beery, D.; Zhou, Y.; Lin, X.; Su, Y.-F.; Xin, Y.; Ma, B. Hollow Metal Halide Perovskite Nanocrystals with Efficient Blue Emissions. *Sci. Adv.* **2020**, 6, eaaz5961.
- (38) Li, H.; Qin, Y.; Shan, B.; Shen, Y.; Ersan, F.; Soignard, E.; Ataca, C.; Tongay, S. Unusual pressure-driven phase transformation and band renormalization in 2D vdW hybrid lead halide perovskites. *Advanced Materials* **2020**, 32, 1907364.
- (39) Lei, L.; Seyitliyev, D.; Stuard, S.; Mendes, J.; Dong, Q.; Fu, X.; Chen, Y.-A.; He, S.; Yi, X.; Zhu, L.; others Efficient energy funneling in quasi-2D perovskites: from light emission to lasing. *Advanced Materials* **2020**, 32, 1906571.
- (40) Walters, G.; Sutherland, B. R.; Hoogland, S.; Shi, D.; Comin, R.; Sellan, D. P.; Bakr, O. M.; Sargent, E. H. Two-Photon Absorption in Organometallic Bromide Perovskites. *ACS Nano* **2015**, 9, 9340–9346.
- (41) Yu, J.; Luo, M.; Lv, Z.; Huang, S.; Hsu, H.-H.; Kuo, C.-C.; Han, S.-T.; Zhou, Y. Recent Advances in Optical and Optoelectronic Data Storage Based on Luminescent Nanomaterials. *Nanoscale* **2020**, 12, 23391–23423.
- (42) Zhuang, Y.; Ren, X.; Che, X.; Liu, S.; Huang, W.; Zhao, Q. Organic Photoresponsive Materials for Information Storage: a Review. *Adv. Photon.* **2020**, 3, 014001.

- (43) Zou, C.; Zheng, J.; Chang, C.; Majumdar, A.; Lin, L. Y. Nonvolatile rewritable photomemory arrays based on reversible phase-change perovskite for optical information storage. *Advanced Optical Materials* **2019**, *7*, 1900558.
- (44) Minh, D. N.; Nguyen, L. A. T.; Trinh, C. T.; Oh, C.; Eom, S.; Vu, T. V.; Choi, J.; Sim, J. H.; Lee, K.-G.; Kim, J.; others Low-Dimensional Single-Cation Formamidinium Lead Halide Perovskites (FAM+ 2PbmBr3m+ 2): From Synthesis to Rewritable Phase-Change Memory Film. *Advanced Functional Materials* **2021**, *31*, 2011093.
- (45) Kanwat, A.; Ghosh, B.; Ng, S. E.; Rana, P. J.; Lekina, Y.; Hooper, T. J.; Yantara, N.; Kovalev, M.; Chaudhary, B.; Kajal, P.; others Reversible photochromism in 110° oriented layered halide perovskite. *ACS nano* **2022**, *16*, 2942–2952.

Supporting Information:

“Photoinduced transition from quasi-2D Ruddlesden-Popper to 3D halide perovskites for optical writing multicolor and light-erasable images”

Sergey S. Anoshkin,[†] Ivan I. Shishkin,[†] Daria I. Markina,[†] Lev S. Logunov,[†]
Hilmi Volkan Demir,^{‡,¶} Andrey L. Rogach,[§] Anatoly P. Pushkarev,^{*,†} and Sergey
V. Makarov^{*,†,||}

[†]*ITMO University, Kronverkskiy pr. 49, 197101 St. Petersburg, Russia*

[‡]*UNAM-Institute of Materials Science and Nanotechnology, Bilkent University, Ankara,
06800, Turkey*

[¶]*School of Materials Science and Engineering, Nanyang Technological University,
Singapore 639798*

[§]*Department of Materials Science and Engineering and Centre for Functional Photonics
(CFP), City University of Hong Kong, 83 Tat Chee Avenue, Kowloon, Hong Kong SAR
999077, P. R. China*

^{||}*Qingdao Innovation and Development Center, Harbin Engineering University, Qingdao
266000, Shandong, P. R. China*

E-mail: anatoly.pushkarev@metalab.ifmo.ru; s.makarov@metalab.ifmo.ru

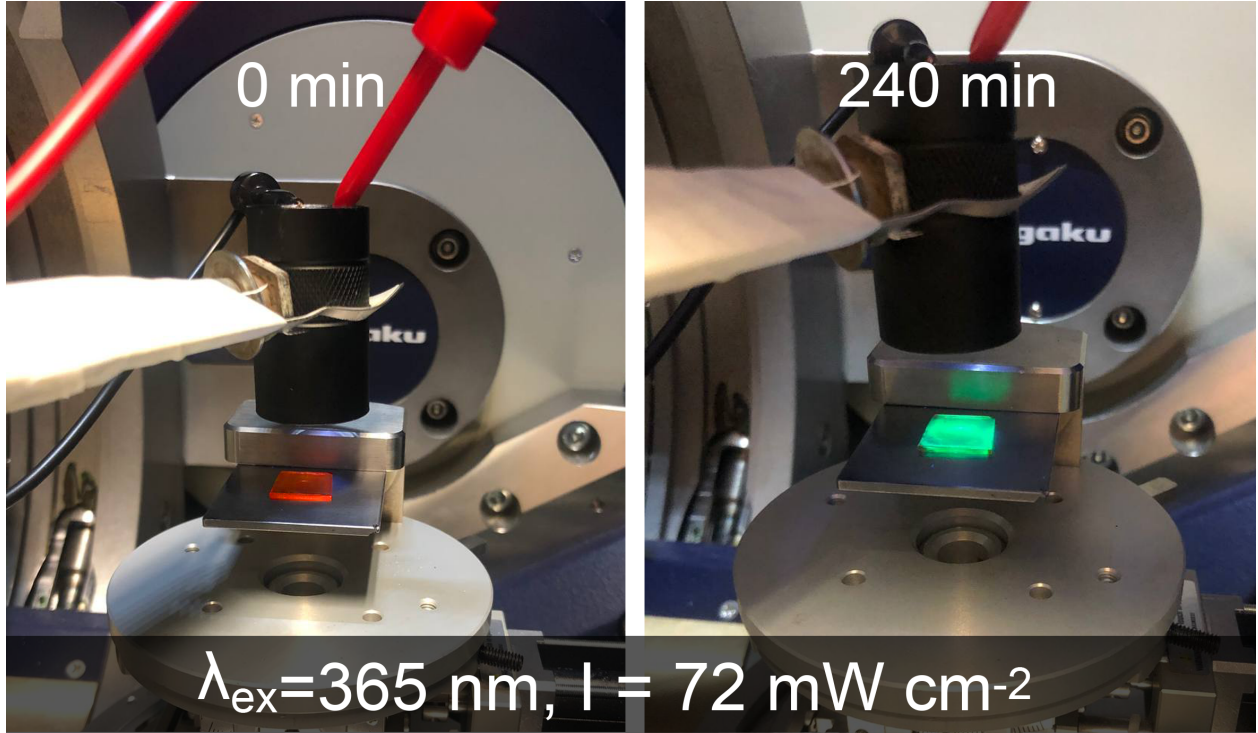


Figure S 1: Photographs of the $n = 3$ quasi-2D perovskite film under continuous-wave UV illumination taken at the beginning and end of *in situ* XRD measurement.

To estimate band gap values for $\text{BA}_2\text{MA}_{n-1}\text{Pb}_n\text{Br}_{n+1}\text{I}_{2n}$ ($n = 1-3$) phases the deconvolution of their absorption spectra $\alpha(h\nu)$ is done (Fig. S2a,c,e). For an adequate approximation of excitonic absorption, we employ the following function describing a sum of discrete excitonic peaks:

$$\alpha(h\nu) \propto \frac{1}{h\nu} \left[\sum_j \frac{2E_b}{j^3} \text{sech} \left(\frac{h\nu - E_g + \frac{E_b}{j^2}}{\Gamma} \right) \right] \quad (1)$$

where E_g denotes the band gap, E_b - exciton binding energy, Γ stands for spectral broadening of exciton, and j takes integer values from 1 to 3. A signal compensation before the band-to-band absorption cutoff is obtained when the fitting parameters are adjusted as follows:

- i) for $n = 1$, $\Gamma = 0.11$ eV, $E_b = 0.22$ eV, $E_g = 2.98$ eV;
- ii) for $n = 2$, $\Gamma = 0.07$ eV, $E_b = 0.17$ eV, $E_g = 2.62$ eV;
- iii) for $n = 3$, $\Gamma = 0.06$ eV, $E_b = 0.15$ eV, $E_g = 2.45$ eV.

The residual signal in the spectra describes band-to-band absorption and can be further used for obtaining corresponding Tauc plots (Fig. S2b,d,f). By extrapolating a linear region

of $[\alpha h\nu]^2(h\nu)$ curves to the abscissa ($[\alpha h\nu]^2=0$) the same values of band gaps are derived.

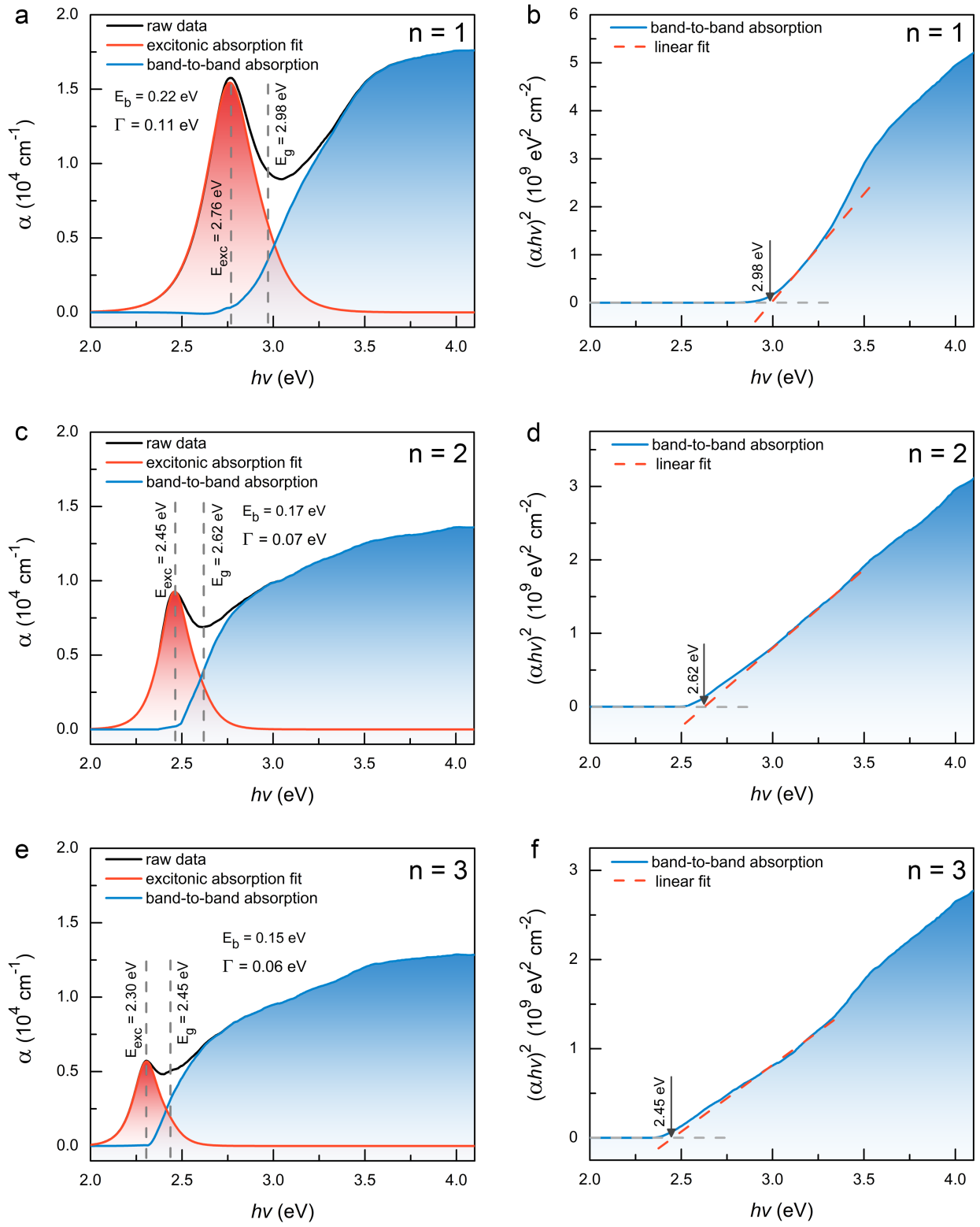


Figure S 2: (a,c,e) Deconvolution of absorption spectra for $n = 1$ (a), $n = 2$ (c), and $n = 3$ (e) thin films. (b,d,f) Tauc plots for $n = 1$ (b), $n = 2$ (d), and $n = 3$ (f) thin films.

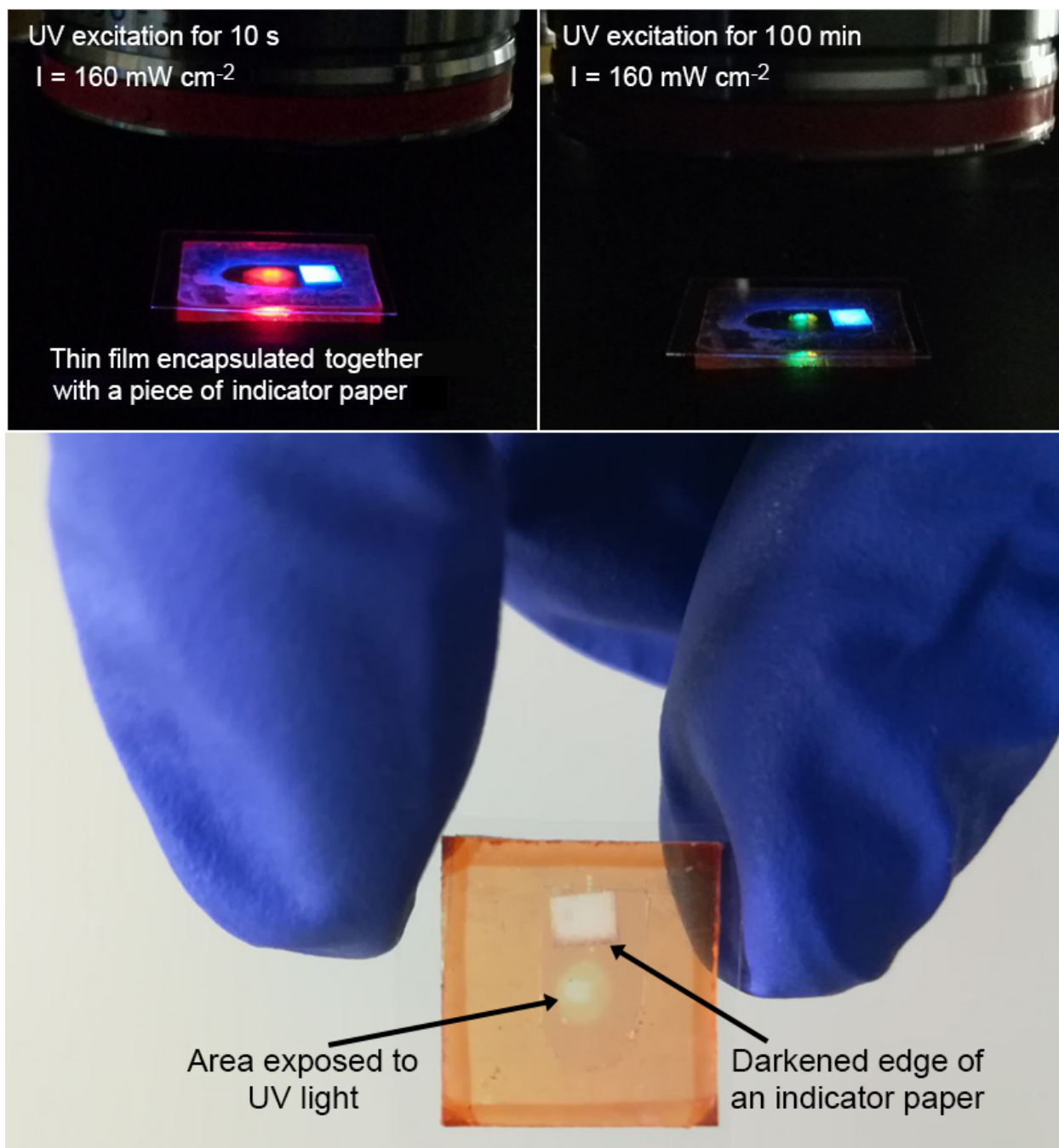


Figure S 3: Photographs of the $n = 3$ quasi-2D perovskite film sealed together with a piece of potassium iodide indicator paper upon focused continuous-wave UV excitation with intensity of 160 mW cm^{-2} for 10 s (left top image) and for 100 min (right top image). Bottom picture reveals a darkened edge of the indicator paper beside the exposed area of the film, proving I_2 species release during the illumination procedure.

$\lambda_{\text{ex}} = 360 \text{ nm}$, $I = 160 \text{ mW cm}^{-2}$

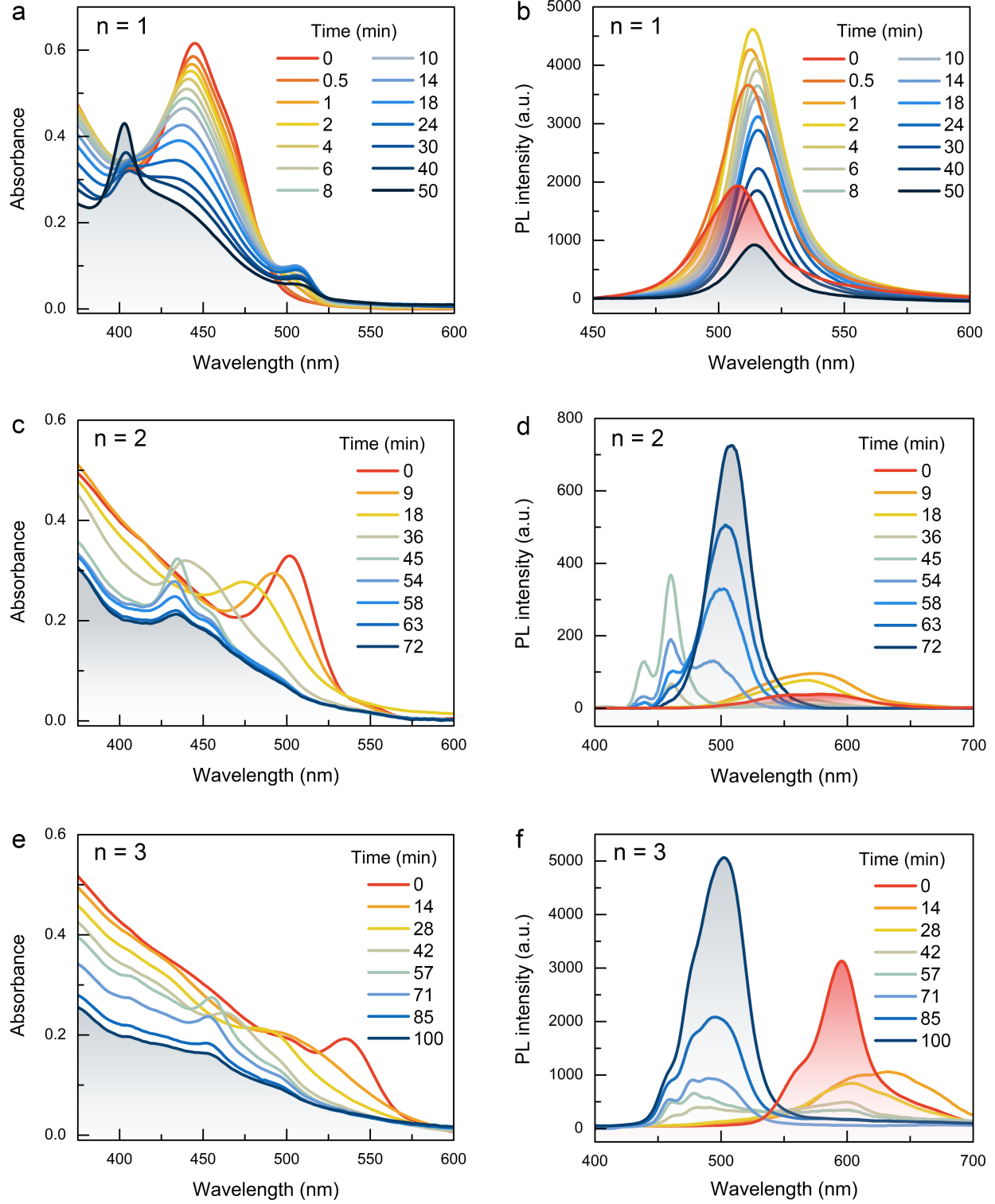


Figure S 4: Absorption and PL dynamics for $n = 1-3$ films exposed to UV light.

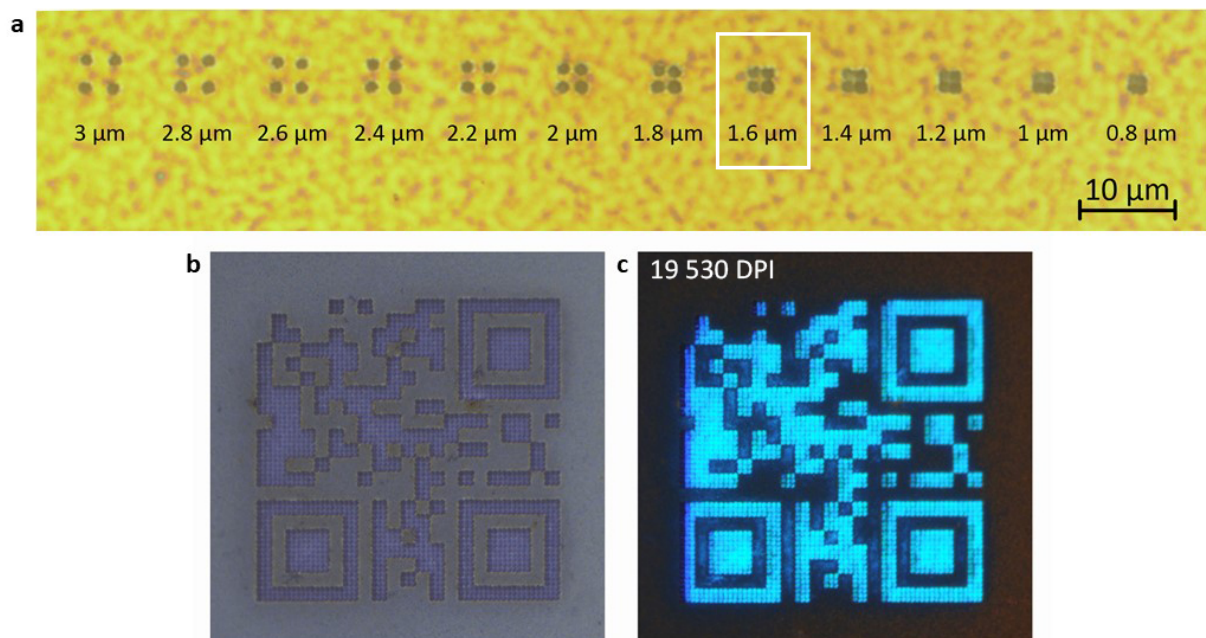


Figure S 5: (a) A bright-field image of a set of 2×2 dots patterns on the $n = 3$ quasi-2D perovskite film obtained on a direct laser writing setup. A dimension in μm below each pattern indicates the distance between the centers of $1 \mu\text{m}$ diameter dots. A white box defines the pattern demonstrating the best spatial resolution of 19,500 DPI. (b,c) High-resolution bright-field and fluorescent microimages of the QR code produced by using two-photon direct laser writing method.

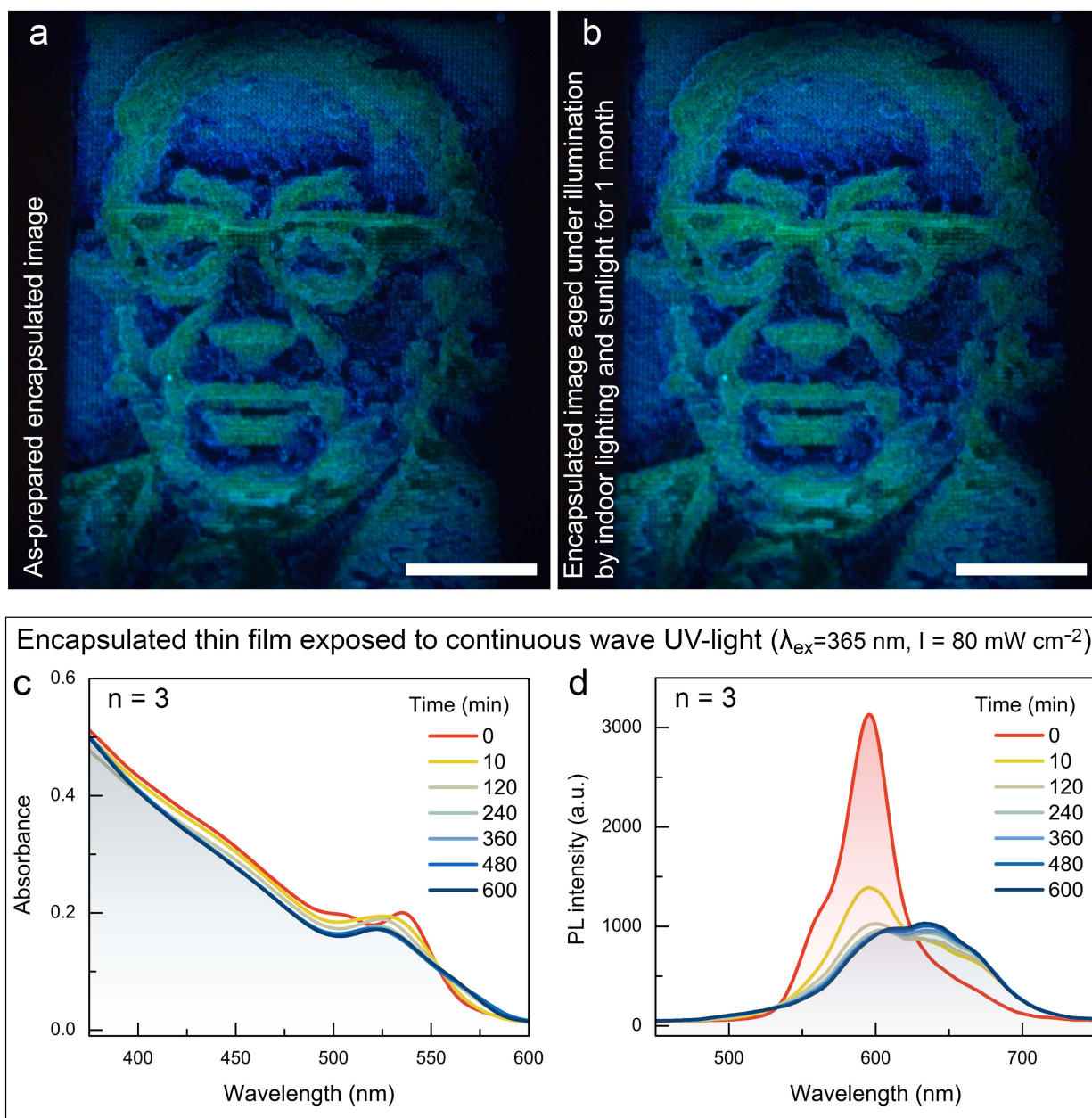


Figure S 6: (a,b) Pictures of an as-prepared (a) and aged (b) luminescent microimage encapsulated at ambient conditions (scale bar is 50 μm). (c,d) Absorption and PL spectral dynamics for $n = 3$ film encapsulated at ambient conditions and then exposed to UV light for 600 min.

Continuous wave UV-light excitation of a thin film encapsulated together with
KI test paper masked by aluminum foil

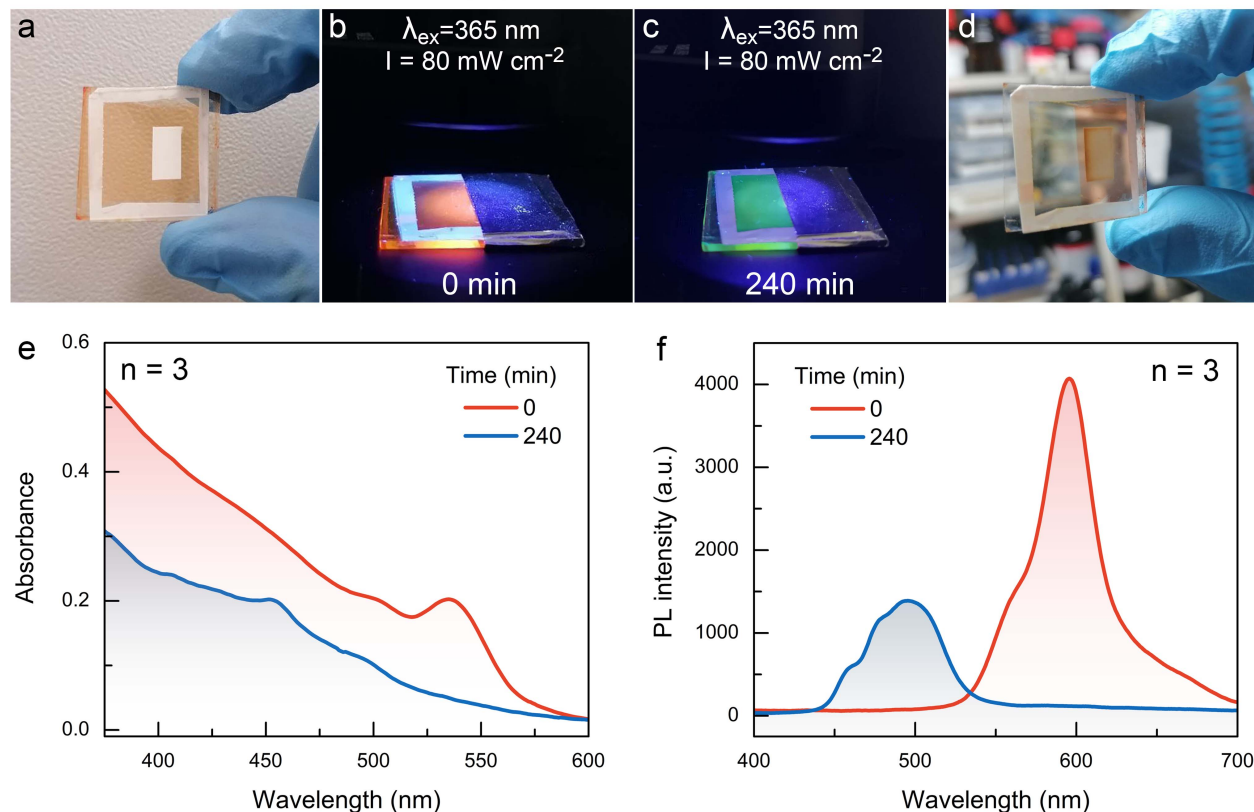


Figure S 7: (a) Picture of $n = 3$ film encapsulated together with KI test paper in a N_2 -filled glovebox. (b,c) Pictures showing PL color for a non-masked area of the film at the beginning of the UV-light exposure procedure (b) and after 240 min of continuous illumination (c). KI test paper is masked by aluminum foil. (d) Picture presenting a bleached part of the film along with a dark edge of the test paper as a result of the release of I_2 species from the former and their absorption by the latter. (e,f) The change in the absorption and PL spectra for the non-masked area of the film at the beginning of the UV-light exposure procedure and at its end.